Martensitic transition near room temperature and the temperature- and magnetic-field-induced multifunctional properties of $Ni_{49}CuMn_{34}In_{16}$ alloy

V. K. Sharma, M. K. Chattopadhyay, A. Khandelwal, and S. B. Roy*
Magnetic and Superconducting Materials Section, Raja Ramanna Centre for Advanced Technology, Indore 452013, India
(Received 23 July 2010; published 23 November 2010)

A near room-temperature martensitic transition is observed in the ferromagnetic austenite state of $Ni_{50}Mn_{34}In_{16}$ alloy with 2% Cu substitution at the Ni site. Application of magnetic field in the martensite state induces a reverse martensitic transition in this alloy. dc magnetization, magnetoresistance and strain measurements in this alloy reveal that associated with this martensitic transition there exist a large magnetocaloric effect, a large magnetoresitance and a magnetic-field temperature-induced strain. This NiMnIn alloy system thus is an example of an emerging class of magnetic materials whose physical properties can be tuned by suitable chemical substitutions, to achieve magnetic-field and temperature-induced multifunctional properties at and around room temperature

DOI: 10.1103/PhysRevB.82.172411 PACS number(s): 75.30.Kz, 81.30.Kf

I. INTRODUCTION

Martensitic transition is a first-order solid-state diffusionless phase transition from high-temperature austenite (AST) phase to low-temperature martensite (MST) phase.[1] This transition has drawn much attention since 1930s, when it was found to be instrumental in conferring an outstanding combination of strength and toughness in steels. Since then many materials, which include nonferrous alloys, metals, ceramics, minerals, inorganic compounds, and polymers are known to exhibit martensitic transition. In 1970s The influence of this transition came into limelight in another area when one-to-one correspondence between shape memory effect and thermoelastic martensitic transition was unambiguously demonstrated in a Cu-Ni-Al shape-memory alloy.[2] Further, in 1990s it was discovered that a field-induced variant reorientation took place in the MST phase of NiMnGa-based Heusler alloys, which gave rise to magnetic shape-memory effect.[3]

In recent times the ternary off-stoichiometric Heusler alloy system $Ni_{50}Mn_{50-x}In_x$ has drawn much attention because of their interesting functional properties such as ferromagnetic shape-memory effects,[4–6] magnetic superelasticity,[7] magnetocaloric effect,[7–10] magnetoresistance,[11,12] large magnetothermal conductivity,[13,14] and barocaloric effect.[15] The key to these functionalities except in the case of barocaloric effect is a temperature- and magnetic-field-induced martensitic transition.[16] The role of the magnetic field is played by hydrostatic pressure in the case of barocaloric effect.[15] In most of these NiMnIn Heusler alloys the martensitic transition takes place in the temperature regime below room temperature, thus limiting the scope of technological applications. Few exceptions are $Ni_{45}Co_5Mn_{36.7}In_{13.3}$,[17] $Ni_{50}Mn_{34.8}In_{15.2}$,[18] and $Ni_{51}Mn_{32.8}In_{16.2}$ (Ref. 19) alloys showing a martensitic transition around room temperature. A large magnetocaloric effect and magnetic-field-induced shape recovery has been observed in $Ni_{45}Co_5Mn_{36.7}In_{13.3}$ due to reverse martensitic transition at 292 and 298 K, respectively.[17] Thus a definite direction to obtain NiMnIn alloys with room temperature or near room-temperature martensitic transition, remains a subject of active research.

In NiMnIn and other NiMnZ (Z=Ga, Sn, Sb) Heusler alloys the magnetic moments are assumed to be localized at Mn atoms which are magnetically coupled through conduction electron-mediated oscillatory exchange interaction.[20,21] Many of these Heusler alloys undergo a transition from paramagnetic (PM) AST phase to ferromagnetic (FM) MST phase with the decrease in temperature. In the MST phase of some of these Heusler alloys with off-stoichiometric composition, the PM-FM transition is followed by a martensitic transition at a further lower temperature.[16] There is a significant decrease in magnetization in the MST phase, and this is presumably due to closer neighbor Mn-Mn positions in the MST phase, which become antiferromagnetically coupled. For some alloy composition of NiMnIn family even a paramagnetic MST phase has been reported.[22] A deeper insight on the martensitic transition in $Ni_2Mn_{1+x}Sn_{1-x}$ has been obtained in a very recent study with the help of x-ray photoelectron spectroscopy and a first-principles density-functional calculation.[23] An abrupt decrease in the peak associated with Ni 3d e_g states is observed at the martensitic transition for the alloys with composition x=0.36–0.42. It is argued that the energy shift of the Ni minority spin e_g state in the AST phase took place due to the hybridization with the antiferromagnetically coupled Mn in the Sn site.[23] It was further stated that the Jahn-Teller splitting of the Ni 3d e_g states played an important role in driving the instability of the cubic AST phase for $X \geq 0.36$ (Ref. 23). This idea of the important role of hybridization of Ni 3d states and 3d states of antiferromagnetically coupled Mn atoms at the Sn sites, has motivated us to study the effect of substitution of Cu atoms at the Ni site of NiMnIn alloys exhibiting martensitic transition. The $3d^{10}$ states of Cu atoms are likely to enhance the extent of hybridization in such alloy systems. Here we show that a small amount (2 at. %) of Cu substitution for Ni atoms indeed causes a large shift of martensitic transition in $Ni_{50}Mn_{34}In_{16}$ from 240 to 295 K. This martensitic transition in turn leads to large magnetocaloric effect, large magnetoresistance and a magnetic-field temperature-induced strain in this Cu-doped $Ni_{50}Mn_{34}In_{16}$ alloy.

A polycrystalline sample with nominal composition of $Ni_{49}Cu_1Mn_{34}In_{16}$ was prepared by arc melting under argon atmosphere. The sample was characterized with x-ray diffraction (XRD) study performed with a PANalytical X-Pert

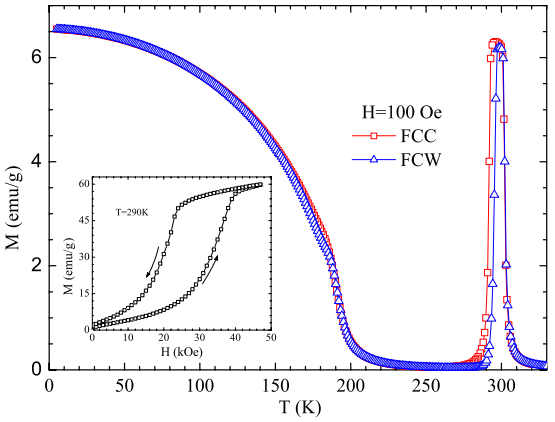

FIG. 1. (Color online) Magnetization vs temperature plot for NiCuMnIn alloy obtained with an applied field of 100 Oe in FCC and FCW modes. The inset shows the isothermal magnetization vs field plot for the same alloy at 290 K.

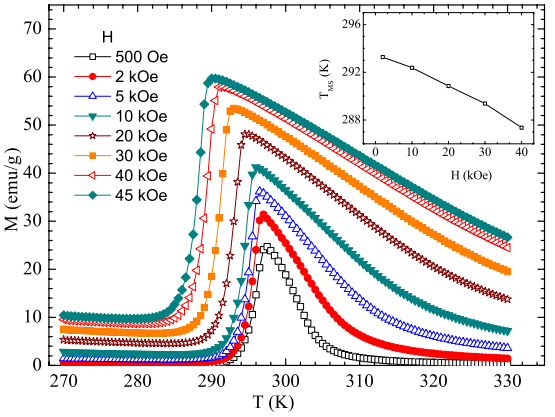

FIG. 2. (Color online) Magnetization vs temperature plot for NiCuMnIn alloy at various temperatures obtained in the ZFC mode. The inset shows the onset temperature of martensitic transition T_{MS} while cooling as a function of applied magnetic field.

PRO MRD machine and energy dispersive x-ray (EDX) analysis using a Philips XL-30pc machine. The sample was found to be homogeneous with average composition $Ni_{48.3}Cu_{0.9}Mn_{33.9}In_{16.9}$. In the rest of the Brief Report this alloy will be presented as NiCuMnIn. The parent alloy $Ni_{50}Mn_{34}In_{16}$, with which the present alloy system will be compared, will be termed as NiMnIn. Room-temperature XRD pattern shows presence of two phases in the NiCuMnIn alloy, which arises due to an admixture of austenite and martensite phases. (The study of various physical properties described below indeed shows evidence of a austenite to martensite phase transition around room temperature.) The AST phase with $L2_1$ ordering has a lattice constant of 6.01 A^0. The MST phase with orthorhombic structure has lattice constants $a=17.67$ A^0, $b=10.78$ A^0, and $c=4.62$ A^0, respectively. dc magnetization measurements were performed using a superconducting quantum interference device magnetometer (Quantum Design). The magnetoresistance measurements between 5 and 300 K were carried out in a 50 kOe multipurpose magnet cryostat system using a superconducting magnet (American Magnetics). Temperature and magnetic-field-dependent strain measurements along the direction of applied magnetic field, were performed with strain gauges in the same magnet cryostat system. Differential measurement of relative length change $\Delta L/L$ was carried out using copper as reference material.

The main frame of Fig. 1 presents magnetization (M) versus temperature (T) plots for NiCuMnIn obtained in the field-cooled-cooling (FCC) and field-cooled-warming (FCW) modes in an applied field of $H=100$ Oe. In FCC mode, measurement is made while cooling the sample from above 320–5 K in the presence of an applied H. After reaching 5 K the sample is warmed up again in the same H and this is called the FCW mode. The sharp rise in $M(T)$ while cooling down with a point of inflection around 300 K, is attributed to the PM to FM transition. Around 295 K, $M(T)$ undergoes a very sharp drop and this marks the onset of martensitic transition in this alloy system. This martensitic transition is accompanied by distinct thermal hysteresis between $M_{FCC}(T)$ and $M_{FCW}(T)$, which highlights the first order nature of this martensitic transition. On the other hand, the PM to FM transition (which takes place entirely within the AST phase) is second order in nature, as is evidenced by the absence of any thermal hysteresis. The magnetization acquires a very low value in the MST phase in the T regime just below the martensitic transition point. This is suggestive of the paramagnetic or antiferromagnetic nature of the MST phase in this T regime. M increases with lowering in T and inverse susceptibility (H/M) in the T regime 245–215 K shows a linear T dependence. Such a behavior is usually a characteristic of paramagnetic phase in a material and not expected in the antiferromagnetic phase. With further decrease in T a ferromagnetic transition takes place in the MST phase around 190 K (see Fig. 1). The existence of the spontaneous magnetization in the T regime below 190 K has been confirmed through the study of Arrott plots. In the inset of Fig. 1 we plot isothermal magnetization (M) vs field (H) plot at 290 K. This M-H plot shows a clear evidence of magnetic-field-induced reverse martensitic transition. This in turn suggests the potential of this system for large magnetocaloric effect, large magnetoresistance, and field-induced strain. We shall now probe below systematically all these possibilities.

The main frame of Fig. 2 presents M vs T plots for the NiCuMnIn alloy in various applied H up to 45 kOe concentrating mainly on the martensitic transition. These M vs T plots were obtained in the ZFC mode starting each time from a temperature well inside the MST phase. With the increase in H the martensitic transition temperature is clearly lowered. Isothermal entropy change ΔS induced by applied H is usually estimated from isothermal M vs H plots by numerical integration of thermodynamical Maxwell relation. However, there are some serious reservations about using this method in the case of a first-order magnetostructural transition.[24,25] Hence we have used the following equation to determine the entropy change $\Delta(S)$:

$$\Delta S(T,H) = S(T,H) - S(T,0) = \mu_0 \int_0^H \left[\frac{\delta M(T)}{\delta T} \right]_H dH. \quad (1)$$

The numerical integration of $(\frac{\delta M(T)}{\delta T})$ is performed using a set of M vs T plots obtained with different applied H of closely

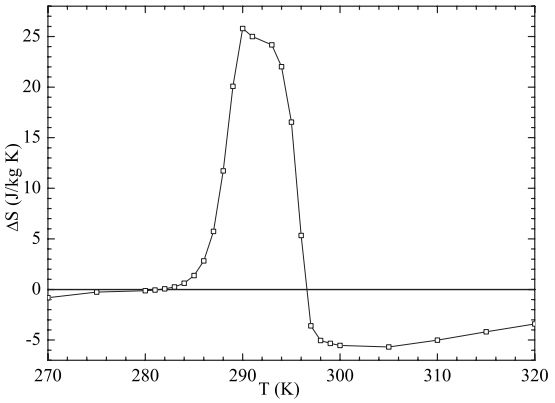

FIG. 3. Change in entropy ΔS versus temperature plot in the NiCuMnIn sample obtained with an applied field of 45 kOe.

spaced values (see Fig. 2; results exist for many other applied H values but not shown here for the sake of clarity). Figure 3 shows the estimated ΔS as a function of T in an applied H of 45 kOe. The inverse magnetocaloric effect peaks around 292 K with a value of 25.8 J/kg K. This is considerably larger than peak value of 19 J/kg K observed in the parent alloy NiMnIn around 240 K in an applied field of 80 kOe.[8] We have further crosschecked the value of ΔS in NiCuMnIn alloy by estimating it from the martensitic transition temperature T_{MS} versus H plot (see inset of Fig. 2) using Clausius-Clapeyron equation. Here we identify T_{MS} from the M-T plots as the temperature of onset of the MST phase while cooling. Taking the difference between magnetizations of austenite and martensite phases at $H=45$ kOe $\Delta M \approx 50$ emu/gm and the value of slope (as deduced from the T_{MS} versus H plot) $dH/dT \approx 5.3$ kOe/K, the estimated value of $\Delta S=26.5$ J/kg K. This peak value of magnetocaloric effect in the present NiCuMnIn alloy can be compared with the $\Delta S=28.4$ J/kg K in $Ni_{45}Co_5Mn_{36.7}In_{13.3}$ alloy observed around 292 K.[17] This value in the later case was estimated from Maxwell's equation using the isothermal M-H curves with a maximum applied field of 70 kOe.

Figure 4 shows the temperature dependence of electrical resistance between 5 and 300 K obtained in the ZFC and FCC mode in applied H of 0 and 50 kOe. The sharp rise in the resistance around 295 K while cooling marks the onset of martensitic transition, which agrees well with that determined from magnetization measurements. The distinct thermal hysteresis between the heating and cooling resistance curves again emphasizes the first-order nature of the martensitic transition. The applied H causes the martensitic transition to take place at a lower T and this gives rise to large negative magnetoresistance. The inset of Fig. 4 shows the magnetoresistance $MR=(\frac{R(H)-R(0)}{R(0)})$ as a function of H at $T=290$ K. The magnetoresistance (MR) reaches a maximum value of 50%. This can be compared with the peak value of MR=64% observed in the parent NiMnIn alloy around 230 K with same maximum applied H of 50 kOe.[11]

Figure 5 present the results of temperature dependent strain $(\Delta L/L)$ measurement in NiCuMnIn alloy in $H=0$ and 40 kOe. $\Delta L/L$ increases with increasing T starting from well inside the MST phase in zero magnetic field and shows a small dip at 293 K followed by a sharp rise of about 0.08%

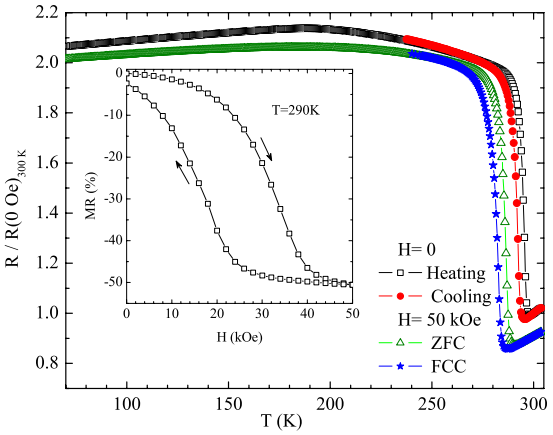

FIG. 4. (Color online) Resistance versus temperature plot in 0 and 50 kOe field obtained in the ZFC and FCC modes. The value of resistance is normalized with respect to the resistance in zero magnetic field at 300 K. The inset shows isothermal MR versus magnetic field plot at $T=290$ K.

at 296 K. Thereafter it continues to increase smoothly with further increase in T. A similar behavior is seen on decreasing T from well inside the AST phase with a distinct thermal hysteresis between 292 and 298 K. In line with the results of magnetization and resistance measurements we attribute this sharp change in $\Delta L/L$ and the associated thermal hysteresis with the martensitic transition in NiCuMnIn alloy.

In an earlier study on various Ni-Mn-based Heusler alloys it was observed that the martensitic transition temperature increased linearly with the increase in the valence electron concentration (e/a).[26] The actual composition of the present NiCuMnIn alloy is $Ni_{48.3}Cu_{0.9}Mn_{33.9}In_{16.9}$ and accordingly the e/a ratio of this alloy composition is 7.81. This value is slightly lower than the estimated value of $e/a=7.86$ for the parent $Ni_{50}Mn_{34}In_{16}$. Accordingly the martensitic transition temperature in this NiCuMnIn alloys should have been marginally lower, which is in contradiction to the observed experimental results. On the other hand, in line with the recent study on the NiMnSn alloys,[23] the increased martensitic tran-

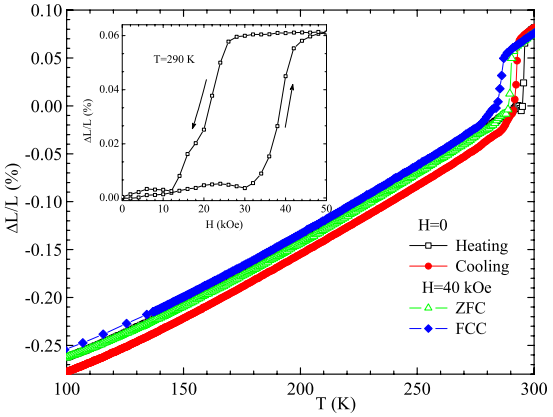

FIG. 5. (Color online) Strain $(\Delta L/L)$ versus temperature plot in 0 and 40 kOe field obtained in the ZFC and FCC modes. The inset shows isothermal strain $(\Delta L/L)$ vs magnetic field plot at $T=290$ K.

sition temperature can be attributed to the enhanced hybridization of 3*d* states at the Ni sites and 3*d* states of antiferromagnetically coupled Mn atoms at the In sites. Accordingly we suggest that the enhanced hybridization originating from the Cu doping at the Ni site is the primary cause of the increase in the martensitic transition temperature from 240 K in the parent NiMnIn alloy to near room temperature in the present NiCuMnIn alloy. We hope that the present work will stimulate a photoelectron spectroscopy study in the present NiCuMnIn alloy to prove this conjecture.

In conclusion we have shown that the small substitution of Cu in the Ni site of $Ni_{50}Mn_{34}In_{16}$ raises the martensitic transition from 240 to 295 K. This martensitic transition in NiCuMnIn alloy gives rise to multifunctional properties, namely, magnetocaloric effect, magnetoresistance, and magnetic-field-induced strain near room temperature. We conjecture that the enhanced hybridization of 3*d* states at the Ni sites and 3*d* states of antiferromagnetically coupled Mn atoms at the In sites, is the primary cause of the increase in the martensitic transition temperature of the present NiCuMnIn alloy. The present result will hopefully provide a direction in the search of NiMn-based Heusler alloys with multifunctional properties at room temperature.

ACKNOWLEDGMENTS

The authors acknowledge the experimental help of R. K. Meena, A Chouhan, A Sarkar, T Ganguli, Ravi Kumar, P Tiwari, P Mondal, and S Nath.

*sbroy@rrcat.gov.in

[1] P. Haasen, *Physical Metallurgy* (Cambridge University Press, Cambridge, 1997).
[2] T. Tadaki, K. Otsuka, and M. Simizu, Annu. Rev. Mater. Sci. **18**, 25 (1988), and references therein.
[3] K. Ullakko, J. K. Huang, C. Kantner, R. C. O'Handley, and V. V. Kokorin, Appl. Phys. Lett. **69**, 1966 (1996).
[4] Y. Sutou, Y. Imano, N. Koeda, T. Omori, R. Kainuma, K. Ishida, and K. Oikawa, Appl. Phys. Lett. **85**, 4358 (2004).
[5] K. Oikawa, W. Ito, Y. Imano, Y. Sutou, R. Kainuma, K. Ishida, S. Okamoto, O. Kitakami, and T. Kanomata, Appl. Phys. Lett. **88**, 122507 (2006).
[6] T. Krenke, M. Acet, E. F. Wassermann, X. Moya, L. Manosa, and A. Planes, Phys. Rev. B **73**, 174413 (2006).
[7] T. Krenke, E. Duman, M. Acet, E. F. Wassermann, X. Moya, L. Manosa, A. Planes, E. Suard, and B. Ouladdiaf, Phys. Rev. B **75**, 104414 (2007).
[8] V. K. Sharma, M. K. Chattopadhyay, and S. B. Roy, J. Phys. D **40**, 1869 (2007).
[9] A. K. Pathak, M. Khan, I. Dubenko, S. Stadler, and N. Ali, Appl. Phys. Lett. **90**, 262504 (2007).
[10] X. Moya, L. Mañosa, A. Planes, S. Aksoy, M. Acet, E. F. Wassermann, and T. Krenke, Phys. Rev. B **75**, 184412 (2007).
[11] V. K. Sharma, M. K. Chattopadhyay, K. H. B. Shaeb, A. Chouhan, and S. B. Roy, Appl. Phys. Lett. **89**, 222509 (2006).
[12] B. M. Wang, L. Wang, Y. Liu, B. C. Zhao, Y. Zhao, Y. Yang, and H. Zhang, J. Appl. Phys. **106**, 063909 (2009).
[13] B. Zhang, X. X. Zhang, S. Y. Yu, J. L. Chen, Z. X. Cao, and G. H. Wu, Appl. Phys. Lett. **91**, 012510 (2007).
[14] L. S. Sharath Chandra, M. K. Chattopadhyay, V. K. Sharma, S. B. Roy, and S. K. Pandey, Phys. Rev. B **81**, 195105 (2010).
[15] L. Mañosa, D. Gonzalez-Alonso, A. Planes, E. Bonnot, M. Barrio, J.-L. Tamarit, S. Aksoy, and M. Acet, Nature Mater. **9**, 478 (2010).
[16] A. Planes, L. Manosa, and M. Acet, J. Phys.: Condens. Matter **21**, 233201 (2009).
[17] R. Kainuma, Y. Imano, W. Ito, Y. Sutou, H. Morito, S. Okamoto, O. Kitakami, K. Oikawa, A. Fujita, T. Kanomata, and K. Ishida, Nature (London) **439**, 957 (2006).
[18] V. V. Khovaylo, T. Kanomata, T. Tanaka, M. Nakashima, Y. Amako, R. Kainuma, R. Y. Umetsu, H. Morito, and H. Miki, Phys. Rev. B **80**, 144409 (2009).
[19] F. X. Hu, J. Wang, J. Shen, B. Gao, J. R. Sun, and B. G. Shen, J. Appl. Phys. **105**, 07A940 (2009).
[20] J. Kubler, A. R. Williams, and C. B. Sommers, Phys. Rev. B **28**, 1745 (1983).
[21] E. Sasioglu, L. M. Sandratskii, and P. Bruno, Phys. Rev. B **70**, 24427 (2004).
[22] R. Y. Umetsu, R. Kainuma, Y. Amako, Y. Taniguchi, T. Kanomata, K. Fukushima, A. Fujita, K. Oikawa, and K. Ishida, Appl. Phys. Lett. **93**, 042509 (2008).
[23] M. Ye, A. Kimura, Y. Miura, M. Shirai, Y. T. Cui, K. Shimada, H. Namatame, M. Taniguchi, S. Ueda, K. Kobayashi, R. Kainuma, T. Shishido, K. Fukushima, and T. Kanomata, Phys. Rev. Lett. **104**, 176401 (2010).
[24] L. Tocado, E. Palacios, and R. Burriel, J. Appl. Phys. **105**, 093918 (2009).
[25] V. Recarte, J. I. Pérez-Landazábal, S. Kustov, and E. Cesari, J. Appl. Phys. **107**, 053501 (2010).
[26] T. Krenke, X. Moya, S. Aksoy, M. Acet, P. Entel, L. Manosa, A. Planes, Y. Elerman, A. Yusel, and E. F. Wassermann, J. Magn. Magn. Mater. **310**, 2788 (2007).